Key Points:

- Three-dimensional characterization of daytime thermospheric gravity waves has been made using collocated optical and radio measurements
- Estimated vertical wavelengths of gravity waves from their horizontal characteristics reasonably match with those measured from digisonde
- Thermospheric neutral winds estimated using measured 3-D gravity wave information show a good match with those measured by MIGHTI

Supporting Information:

Supporting Information may be found in the online version of this article.

Correspondence to:

D. Pallamraju,
raju@prl.res.in

Characterization of Gravity Waves in Three Dimensions in the Daytime Thermosphere Using Combined Optical and Radio Measurements and Estimation of Horizontal Neutral Winds

Sunil Kumar[1,2], Subir Mandal[1,3], and Duggirala Pallamraju[1] [ORCID]

[1]Space and Atmospheric Sciences Division, Physical Research Laboratory, Ahmedabad, India, [2]Indian Institute of Technology, Gandhinagar, India, [3]Now at British Antarctic Survey, Cambridge, UK

Abstract Gravity waves, which are considered omnipresent in the Earth's upper atmosphere, are generally investigated by monitoring the fluctuations in different atmospheric parameters. Here, we report the propagation characteristics of thermospheric gravity waves both in horizontal and vertical directions obtained using collocated optical and radio measurements from Ahmedabad, India for February 2021. The measurements of OI 630.0 nm dayglow emission rates over zenith are used to derive time periods of gravity waves. Wave number analyses of variations in the emission over a large field-of-view have been performed to derive gravity wave scale sizes and propagation characteristics in the horizontal direction. Time periods, horizontal scale sizes, and propagation directions are found to be in the range of 31–125 min, 78–243 km, and 203°–248° from east, respectively. Vertical wavelengths of the gravity waves are obtained from radio measurements and are in the range of 26–247 km. As the gravity wave characteristics are influenced by the ambient neutral winds, the measured gravity wave propagation characteristics in three dimensions have been used as inputs into the gravity wave dispersion relation to estimate the magnitudes of thermospheric horizontal neutral winds. These estimated daytime winds in the direction of wave propagation are found to be in the range of 1–105 ms^{-1}, and they compare well with those measured independently from MIGHTI added HWM14 model-derived winds. The daytime winds estimated by this approach are possibly the first of their kind as obtained from ground-based measurements.

Plain Language Summary Atmospheric gravity waves are mostly generated in the lower atmosphere due to different processes, and they carry energy away from their source regions. Therefore, these waves play a crucial role in the coupling and energetics of the atmosphere. As the neutral density decreases exponentially with height, amplitudes of these waves grow in order to conserve energy. At high altitudes, when the amplitudes become very large, these waves break due to non-linear wave-wave interactions and deposit their energy. Such energy deposition can further give rise to secondary and tertiary gravity waves. In favorable background conditions, these waves can propagate deep into the upper atmosphere and alter the prevailing dynamics. Therefore, the characterization of their spatial and temporal scales in the upper atmosphere is extremely important for a comprehensive understanding of atmospheric dynamics. As neutrals and plasma share the same space in the upper atmosphere, we have used simultaneous observations of both the neutrals and plasma, using ground-based optical and radio measurements, to derive the propagation characteristics of the atmospheric gravity waves in all three dimensions. Further, we have used these parameters to estimate the magnitudes of daytime thermospheric horizontal winds, which are otherwise difficult to obtain from ground-based platforms in daytime.

1. Introduction

Waves of different spatial and temporal scales are known to have a significant influence on the upper atmospheric dynamics as they contribute to the coupling of different regions. Among the different types of waves, the effects of large-scale waves such as planetary waves and tides in the atmosphere are relatively well understood, whereas, the understanding of the dynamics related to the gravity waves is far from complete, more so in the daytime. The gravity waves are mostly generated in the lower atmosphere due to changes in orography (e.g., Alexander, 1996; Smith & Lyjak, 1985), tropospheric convective activities (e.g., Alexander et al., 2000; Sato et al., 1995; Singh & Pallamraju, 2016), and wind shears (e.g., Fritts, 1982, 1984; Pallamraju et al., 2014; Pramitha et al., 2015). Further, these waves can also be generated due to auroral processes over the high-latitudes

(Hocke & Schlegel, 1996; Pallamraju et al., 2001), and equatorial electrojet over the low-latitudes (Pallamraju et al., 2010; Raghavarao et al., 1988), among others. If the background conditions are favorable, these gravity waves can propagate to higher altitudes and significantly contribute to the prevailing dynamics (Fritts & Alexander, 2003). As the wave amplitudes increase with altitude, non-linear wave-wave interactions occur in the mesosphere-lower-thermosphere (MLT), which can lead to the breaking of waves. The deposition of energy resulting from the breaking of these waves accelerates the background mean flow at these altitudes. These can further excite secondary and tertiary waves in the MLT region (e.g., Medvedev & Klaassen, 2000; Vadas et al., 2003; Yigit et al., 2008), which can reach the thermospheric altitudes, where they are potentially dissipated by the molecular viscosity and thermal diffusivity (e.g., Francis, 1973; Pitteway & Hines, 1963; Richmond, 1978; Hickey & Cole, 1988; Vadas, 2007; Vadas & Fritts, 2004). Numerous theoretical simulations and modeling studies on the effects of the lower atmospheric gravity waves on thermospheric dynamics have been reported in the literature (e.g., Vadas, 2007; Vadas & Liu, 2009; Yigit & Medvedev, 2009). Studies have shown that gravity waves effects in the ionosphere-thermosphere are comparable to the ion-drag effects, and they can contribute to the heating or cooling of the thermosphere by up to 170 K-day^{-1} till the peak F-layer altitudes (e.g., Miyoshi et al., 2014; Yiğit & Medvedev, 2009). Hence, a critical knowledge of the temporal and spatial characteristics of these atmospheric gravity waves is essential for a better understanding of the upper atmospheric variability. Propagation features of these atmospheric gravity waves are strongly influenced by background conditions, such as, temperature, neutral density, and winds. The neutral winds control the propagation characteristics of the gravity waves, and as a result, the horizontal/vertical scale sizes of the gravity waves increase/decrease due to the neutral winds flowing in the same direction of gravity wave propagation (e.g., Li & Lu, 2021; Mandal et al., 2019; Mandal & Pallamraju, 2020; Pallamraju et al., 2016; Vadas et al., 2009). Therefore, the horizontal neutral winds and propagation of gravity waves are inter-coupled. Further, these background atmospheric parameters are altered by the variation in the incoming solar radiation in the EUV and X-ray wavelengths. Based on changes in the wave dissipation conditions at thermospheric altitudes, the number of gravity waves in the daytime thermosphere, their vertical propagation speeds, and vertical wavelengths have been shown to increase with an increase in the solar activity (e.g., Laskar et al., 2015; Mandal et al., 2020).

One of the most established methods to characterize these neutral gravity waves in the upper atmosphere is to monitor the fluctuations in the natural airglow emissions. As the propagation of any wave disturbs the density and temperature of the reactants that produce these emissions, they leave their imprint on the variations of these airglow emissions (e.g., Pallamraju et al., 2010; Teitelbaum et al., 1981). Single point photometric measurements of airglow emissions can only provide the information of time periods of these waves, whereas, scale sizes and propagation directions of these waves can be derived using large field-of-view (FOV) imaging measurements (e.g., Lakshmi Narayanan et al., 2010; Shiokawa et al., 2009; Taylor et al., 1995). In the presence of strong solar background brightness in the daytime, observation of these faint dayglow emissions is extremely challenging. However, with the advent of new and innovative optical techniques with a high spectral resolution, such measurements have become possible in the recent past. Some of the results obtained by using high-resolution spectrographs are reviewed by Pallamraju and Chakrabarti (2006). Owing to the large FOV of these spectrographs, it is also possible to obtain gravity wave scale sizes by carrying out wave number analysis (e.g., Karan & Pallamraju, 2017, 2018; Pallamraju et al., 2014, 2016). Combining such analyses in the zonal and meridional directions, horizontal scale sizes of gravity waves can be obtained. Such observations were obtained from three dayglow emissions, namely, OI 557.7, OI 630.0, and OI 777.4 nm that emanate from three different altitudes as reported earlier (Pallamraju et al., 2016).

In the present work, we have derived the horizontal propagation characteristics (time periods, scale sizes, and propagation directions) of thermospheric gravity waves using the large FOV observations of OI 630.0 nm dayglow emission rates from Ahmedabad. Further, we have used the phase delays in the height variations of multiple isoelectron densities, as obtained from a digisonde, to derive the vertical propagation characteristics (time periods, phase speed, and scale sizes) of these waves. In an earlier work, using combined optical and radio measurements, it was shown that the wave features are similar in both these measurements indicating that these are the same waves but observed in different techniques (Mandal et al., 2019). Therefore, in this study, we have used such collocated and simultaneous optical and radio measurements to obtain gravity wave characteristics in three dimensions. Further, as the neutral winds affect the wave propagation, using the measured values of gravity wave parameters in all three dimensions from our study as inputs into the gravity wave dispersion relation, we have estimated the thermospheric neutral wind magnitudes. The estimated winds along the direction of wave

propagation by the present method as reported in this study have been found to compare well with those measured by the Ionospheric Connection Explorer (ICON) satellite.

It is known that the measurements of the daytime thermospheric winds from ground-based instruments are extremely challenging in the presence of background sunlight. Applications of the ground-based Fabry-Perot etalons have been reported in the literature as a means for the measurement of neutral winds (e.g., Burnside et al., 1981; Makela et al., 2013; Meriwether et al., 1986), which are restricted to the nighttime, except the one using a triple etalon system, which is suitable for daytime conditions as well (Gerrard & Meriwether, 2011). Instruments on-board satellites have provided daytime neutral winds measurements (e.g., Englert et al., 2017; Herrero et al., 1988; Shepherd et al., 1993). Thus, to the best of our knowledge, the results obtained on daytime thermospheric winds using three-dimensional gravity wave characteristics obtained from ground-based measurements, as reported in the present study, are the first of their kind.

2. Data Sets

For the present study, we have used (a) the OI 630.0 nm dayglow emissions measured by MISE, (b) ionospheric data from digisonde, (c) thermospheric neutral winds measured by MIGHTI on board the ICON satellite, (d) outputs of winds from the Horizontal Wind Model-14 (HWM14) model, and (e) neutral atmospheric parameters, such as, temperature and mass density from the NRLMSISE model. These data sets used for the duration of 5–19 February 2021 are briefly discussed below.

2.1. OI 630.0 nm Dayglow

Dayglow refers to the naturally occurring atmospheric emissions in the daytime, which are produced from different photochemical reactions that occur in the Earth's upper atmosphere. Temporal variations in their emission rates depend on the temperatures and densities of the reactants, which are affected by wave propagation. Therefore, the fluctuations superposed on the broad variations in these emission rates can be used as a tracer to derive the wave propagation characteristics. In this work, the OI 630.0 nm dayglow emissions, which peak at around 230 km, have been used to study the behavior of the gravity waves. The emission region has a thickness of half-value width of around 100 km. The OI 630.0 nm emission is produced mainly from photoelectron impact excitation of atomic oxygen, photodissociation of molecular oxygen, and dissociative recombination of molecular oxygen ions with ambient electrons (Solomon & Abreu, 1989). We have retrieved the dayglow emission rates at 630.0 nm wavelength using the data obtained from the multi-wavelength imaging spectrograph using echelle grating, MISE (Pallamraju et al., 2013), which is in operation from Ahmedabad, India. MISE is an imaging spectrograph providing high-resolution spectral images over a large FOV (around 140°). To retrieve the dayglow emission rates from the sky images obtained by MISE, we remove the scattering contribution due to the Ring-effect (atmospheric scattering) by considering the scattering in the neighboring Scandium line. Such methodology of extracting dayglow emissions buried in the strong solar background continuum is well-established, details of which have been reported in the literature (Pallamraju et al., 2002, 2013). In this study, we have used dayglow observations within the FOV of 106° (zenith − 57° to zenith + 49°), which corresponds to a spatial distance of around 622 km (355 km away from the zenith in one direction and 267 km in the other). We have restricted ourselves to this FOV to avoid the effects of filling-in due to atmospheric scattering from low-elevation angles. The MISE instrument uses a CCD detector of $1,024 \times 1,024$ pixels. In order to improve the signal-to-noise ratio (SNR), we apply an 8-pixel on-chip binning along the spatial direction of the spectrograph, resulting in the final image size of $1,024 \times 128$. The dark count (0.017 electrons s^{-1} pix^{-1} at $-75°C$) and readout noise (3.3 electrons RMS at the readout frequency of 50 kHz) of this CCD are very small. The readout noise gets reduced further due to the 8-pixel binning in the spatial direction.

2.2. Ionospheric Electron Density

We have used the ionospheric electron density measurements from DPS-4D digisonde located at Ahmedabad. This digisonde is programmed to provide ionograms (frequency vs. height of reflection) in the range of 1–12 MHz at a cadence of 7.5 min. All the ionograms have been manually scaled and the variations in the heights of the isoelectron density contours corresponding to digisonde transmitted frequencies at 5.0, 5.5, and 6.0 MHz have

been used collectively to derive the time periods and vertical wavelengths of the gravity waves present in the ionosphere-thermosphere region.

2.3. Neutral Winds

Measured neutral winds from the Michelson Interferometer for Global High-Resolution Thermospheric Imaging, MIGHTI (Englert et al., 2017), on-board ICON (Immel et al., 2018) satellite are used for comparison with our estimated values. MIGHTI makes use of the Doppler shifts in the observed airglow emissions at OI 557.7 and 630.0 nm to provide wind magnitudes between 90 and 300 km. The wind measurements from MIGHTI cover the spatial region of 12°S to 42°N geographic latitudes. Further, we have used MIGHTI added HWM14 winds, an approach described in Kumar et al. (2022) to estimate the diurnal variation in thermospheric winds at a given location. In this approach the MIGHTI winds are used to provide day-to-day corrections to those provided by the HWM14, which is climatological in nature, thereby yielding the diurnal variation of thermospheric wind at a given location, as briefly described in Section 4.4 below.

3. Data Analyses

In this work, we have used collocated digisonde and optical measurements from Ahmedabad, a low-latitude location in the Indian longitudes. The horizontal and vertical propagation characteristics of the thermospheric gravity waves have been derived using OI 630.0 nm dayglow emission observations over a large FOV and radio measurements, respectively. Detailed analysis methodologies are described in the following sections.

3.1. Estimations of Time Period and Horizontal Propagation Characteristics of Gravity Waves

As discussed above, OI 630.0 nm dayglow emission rates can be obtained over a large spatial distance using the observation by MISE. For the present work, we have carried out a special campaign mode observation, wherein, we have rotated the MISE instrument in orthogonal directions—meridional (north-south) and zonal (east-west); in a way such that the slit through which the light enters the instrument, is oriented in each of the directions for 30 min. Such repeated observations along two orthogonal directions enable us to obtain the gravity wave scale sizes in both meridional and zonal directions over a spatial distance of around 622 km (along the FOV of MISE) for the OI 630.0 nm emission altitude as a function of time. The dayglow emission rates at the zenith, which is common in both these orientations, are used to obtain the diurnal variation of dayglow emissions. Further, we have co-added the images obtained for 5 min and over 21 pixels centered around the zenith to improve the SNR. The diurnal variation of OI 630.0 nm dayglow emission rate on a sample day (5 February 2021) is depicted in Figure 1a. It can be noted that in addition to the broad diurnal variations, there are smaller scale fluctuations, which are understood to be caused by the wave activity that exists in those regions. In order to derive more accurate information on the periodic behavior of these fluctuations in the gravity wave regime, residuals (shown as red-dotted line) have been obtained by subtracting 2 hr running-averaged values (black-dashed line) from the actual dayglow values. Thus, the residuals obtained will contain information on the periodicities smaller than the sub-harmonic of the tidal periods (3 hr). The dayglow data used in this work are non-uniformly sampled in the course of observation on a given day. This unequal spacing of data arises due to different exposure times, presence of clouds in the FOV, on occasions, and lack of data around local noon, when the CCD gets saturated by the direct solar glare. Thus, to carry out spectral analysis of the data, we have used the Lomb-Scargle periodogram (Lomb, 1976; Scargle, 1982) technique, which is capable of yielding frequencies present in the non-uniformly sampled data. The Lomb-Scargle periodogram refers to a generalized form of classical periodogram with properties like, (a) it reduces to a classical periodogram for uniformly sampled data, (b) the resultant periodogram is insensitive to time shifts in the data, and (c) it is identical to results obtained by fitting sinusoidal function to the data and constructing a periodogram from the χ^2 goodness of fit at each frequency (VanderPlas, 2018). The results from such analyses of diurnal variation of dayglow emission rates on 5 February 2021 are shown in Figure 1c, wherein, significant time periods (time periods with power spectral density higher than 90% false alarm limit, FAL or statistical significance level) can be seen. It can be noted that gravity waves of time periods around 37, 66, and 101 min are present on this day. Similarly, gravity wave scale sizes are obtained from the variations in dayglow emission rates along the spatial directions. In this case, data obtained for 10–15 min have been co-added and a 11-pixel running average values have been considered to improve the SNR. As an example,
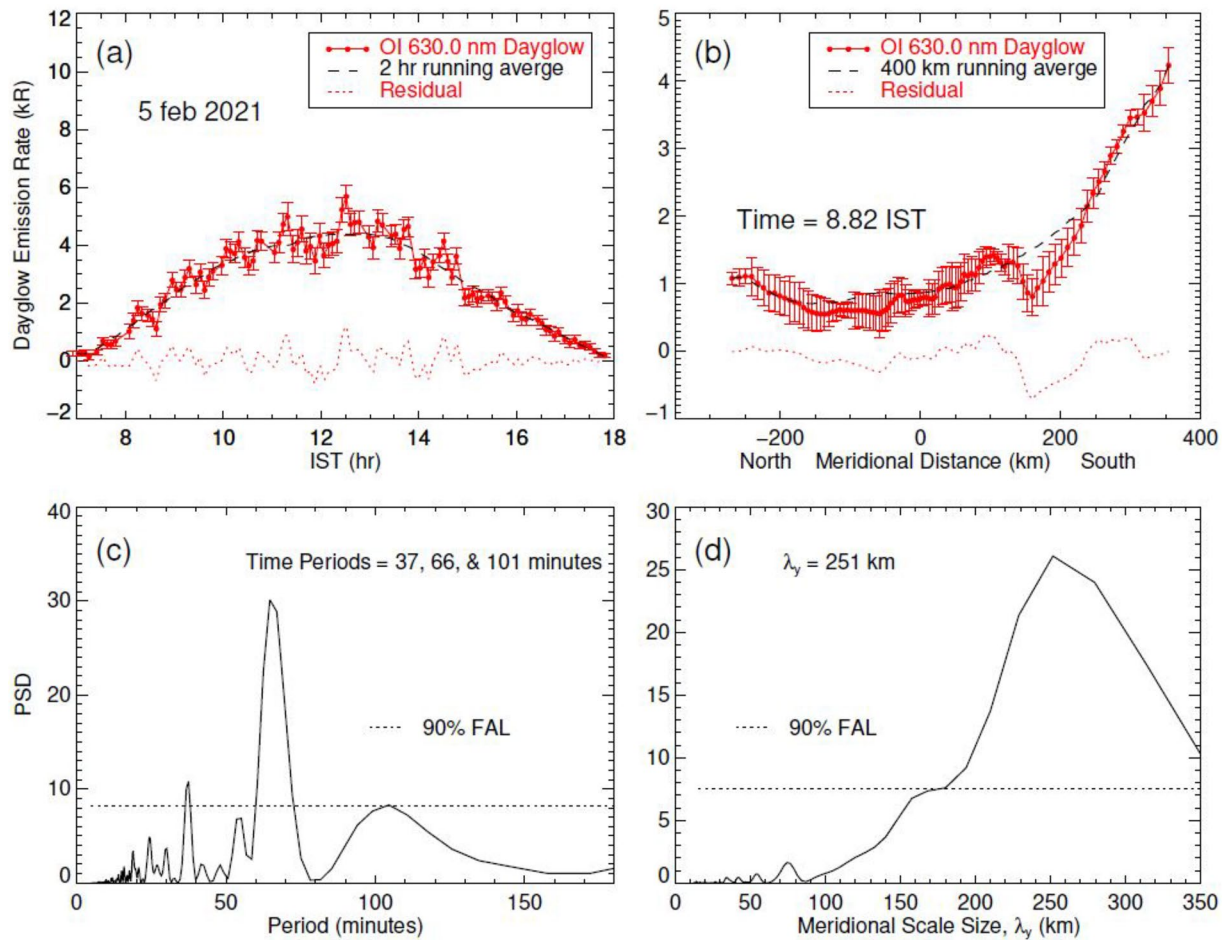
Figure 1. The diurnal variation of the OI 630.0 nm dayglow emissions on a sample day of 5 February 2021 is shown in red-color; black-dashed curve represents 2 hr running averaged values and red-dotted curve is the residual obtained by subtracting the 2 hr running-averaged values from the original values. (b) Variation in the dayglow emission rates at OI 630.0 nm wavelength in the meridional direction corresponding to 8.82 IST; black-dashed line represents 400 km running average dayglow and the residual (obtained by subtracting the running averaged values from original data) is shown by red-dotted line. (c) The Lomb-Scargle periodogram of the residual obtained from the diurnal profile of dayglow is shown in (a), wherein time periods of 37, 66, and 101 min are found to be significant. The black dash-dotted line represents the statistical significance level of 90%. (d) The results from spectral analysis of the residual from meridional dayglow data as presented in (b) are shown here. Presence of a dominant scale size of around 250 km can be seen.

the variations in the dayglow emission rates along the meridional direction at a given time are shown in Figure 1b. The spatial region covered by each pixel is different at different angles, as they vary non-linearly. Over zenith, it is 4 km pixel^{-1} and at the farthest view direction, it is 12 km pixel^{-1}. Thus, considering a 2-pixel separation for estimating the spatial resolution, the maximum uncertainty turns out to be 24 km. Wave number analyses have been carried out on the residual of the spatially varying dayglow emission rates to find the statistically significant scale sizes. The residual is obtained by subtracting 400 km running averaged values from the original data. These residuals are shown by red-dotted line in Figure 1b. Thus, meridional scale sizes (λ_y) of the gravity waves are obtained by performing wave number analysis on data shown in Figure 1b. From Figure 1d, one can see the presence of a meridional scale size of around 251 km on this day at around 8.82 IST. Similarly, we have obtained the zonal scale sizes (λ_x) of gravity waves using the dayglow intensity variation across the zonal direction. In this way, we have obtained the gravity wave scale sizes in the zonal and meridional directions throughout the day. As discussed earlier, the duration of observations in zonal and meridional directions is 30 min each.

Observational evidences have been shown earlier that gravity waves in the thermosphere exist in the form of monochromatic wave packets, that is, they are coherent waves or have similar characteristics throughout the day (e.g., Djuth et al., 2004; Oliver et al., 1994). Further, one wave packet typically lasts around 1–2 hr and has a separation of 20–60 min from another wave packet. In this background, we can safely assume that the gravity

waves observed within 30 min are the same (as the time periods of these gravity waves are 37, 66, and 101 min as shown in Figure 1c). Hence, we have combined the λ_x and λ_y information obtained over 30 min to estimate the horizontal scale sizes (λ_H) of these gravity waves as per the following relation,

$$k_H^2 = k_x^2 + k_y^2 \text{ or } \lambda_H = (\lambda_x \times \lambda_y)/\left(\lambda_x^2 + \lambda_Y^2\right)^{1/2} \tag{1}$$

where k_H, k_x, and k_y are the wave numbers in horizontal, zonal, and meridional directions, respectively.

The derived values of λ_H thus correspond to the time, which is the average of the duration of λ_x and λ_y. We have calculated these values of horizontal scale sizes of gravity waves for all 10 days on which bi-directional observations of OI 630.0 nm dayglow emission are available. Table 1 lists all the time periods of gravity waves obtained from the analyses of dayglow emission rates, and it can be noted that they are greater than 30 min. Therefore, our assumption of considering the scale sizes obtained in orthogonal directions within 30 min to be of the same gravity wave to calculate λ_H is valid for all these days. The diurnal variation of λ_H is shown in Figure 2 for 10 days. In this figure, λ_H is only shown when both λ_x and λ_y are significant (above 90% FAL) in the wave number spectral analysis. Around the local noon, to prevent the saturation of the detector due to direct solar glare, the instrument has been kept in the east-west direction from 12 to 13.5 IST (UT + 5.5 hr). Therefore, for this period, we only have the values of λ_x. The values of λ_y for these times are interpolated by considering the values of λ_y around 12 and 13.5 hr IST (pre- and post-noon time). They have been considered together to estimate the values of λ_H, and are shown by black-dotted lines in Figure 2 to separate them from the other values.

Further, the phase propagation angles (θ_H) of these waves are calculated using the measured λ_x and λ_y since they are related as $\theta_H = \tan^{-1}(\lambda_x/\lambda_y)$. These values of θ_H have a degeneracy of 180°. In order to estimate the propagation direction unambiguously, we have used the methodology described in an earlier study (Pallamraju et al., 2016). In this method, to obtain the spatial location of a dominant scale size at a given time, inverse Fourier transforms have been performed by retaining only the power spectral signal of a given dominant scale size (in the frequency domain) at a time. In doing so the spectral power corresponding to the dominant scale size with a bandwidth of 24 km (which is the uncertainty in the scale sizes as discussed above) is retained and the power of the rest of the scale sizes have been equated to zero. This process is repeated throughout the day for both directions and the results from such an exercise for a representative day (5 February 2021) are shown in Figure 3, wherein, the locations of the wave crests and troughs as a function of time become clearly visible. The y-axis of the left panel shows the wave characteristics in the meridional direction, whereas, the x-axis shows the time in IST. In the right panel, the waves in the zonal direction are shown along the x-axis, and time along the y-axis. One can note the crests and troughs of the gravity wave scale sizes oriented in orthogonal directions in both these panels. The black lines are drawn to trace the crests and troughs of the gravity wave at different times. Thus, they indicate the movement of phase fronts with time which are southward as seen in the left panel, and westward as seen in the right panel. Based on this combined information, it can be inferred that the gravity waves are broadly propagating in the south-west direction on this day. Such analyses have been carried out for all the days and we found that the observed gravity waves are propagating in the south-west directions in this duration. The propagation directions of these waves as described in this method are presented with time in Figure 4 as red-colored dashed arrows for all the 10 days of available bi-directional data that are shown in Figure 2 (the solid black lines are the direction of neutral winds as described below in Section 4.4). Here, the values on the y-axis correspond to the day of the month of February 2021. Such methods have been shown (Hocke & Kampfer, 2009; Pallamraju et al., 2016) to bring out accurate information on the spatio-temporal variations of a given periodic fluctuations. In an earlier work (Mandal & Pallamraju, 2020), by comparing the variations in the vertical speeds of gravity waves as obtained from analyses of digisonde measurements with the variation in the HWM14 model-derived winds, it was inferred that the gravity waves mostly show south-westward propagation in the daytime thermosphere over Ahmedabad. Hence, the horizontal wavelengths and propagation directions of atmospheric gravity waves obtained in the present work in the daytime thermosphere over Ahmedabad are consistent with the earlier findings as well. The horizontal characteristics (time period, λ_x, λ_y, λ_H, and θ_H) of gravity waves on all these 10 days are found to be in the range of 31–138 min, 88–344 km, 123–344 km, 78–243 km, and 203°–248° from the east direction, respectively, and are listed in Table 1.

3.2. Vertical Propagation Characteristics of Gravity Waves

Digisonde-derived height variations of isoelectron densities have been used to obtain the vertical wavelengths of the atmospheric gravity waves present in the thermosphere. The details of deriving vertical scale sizes have

Table 1
Gravity Wave Parameters, Such as, Time Periods in Optical Data, Time Periods in Radio Data, λ_x, λ_y, λ_H, θ_H, Estimated λ_z From Gravity Wave Dispersion Relation Using Horizontal Characteristics of Gravity Waves as Obtained by Optical Measurement, and Measured λ_z From Digisonde are Shown for all the Days.

A	B	C	D	E	F	G	H	I	J
S.No.	Date (in the month of February 2021)	Optical period (minutes)	Radio period (minutes)	Zonal scale size, λ_x (km) from optical data	Meridional scale size, λ_y (km) from optical data	Horizontal scale size, λ_H (km) from optical data	Phase propagation angle, θ_H from optical data	Estimated vertical scale size, λ_Z (km) from Hines, (1960) GW dispersion relation	Measured vertical scale size λ_Z (km) from radio data
1	5 February	37, 66, **101**	**94**	182–281	182–344	128–199	207–232	40–61 19–36 9–25	65–90
2	6 February	33, 53, 65, 126	NVP	206–344	123–344	140–243	208–239	36–109 15–74 9–64 1–44	-
3	7 February	**41**, 55, 66, 99	**41**	88–281	162–344	78–199	207–243	18–72, 13–57, 11–51, 4–40	71–81
4	8 February	**49**, 63, 79, 135	37, **52**, 109	162–344	162–344	115–243	222–237	30–51 21–39 15–31 6–23	51–75 69–82 149–247
5	12 February	**40**, 54, 67, 116	**37**	162–344	182–344	128–199	211–242	34–53 22–39 16–32 3–19	28–36
6	13 February	**31**, 63, **94**, 126	**37**, **104**	147–281	162–344	112–199	203–237	28–72 8–40 2–32 1–28	56–83 85–167
7	14 February	**37**, 56, 65, 138	**37**	147–344	134–281	113–199	221–248	30–56 3–38 1-30 1–26	26–41
8	16 February	37, 90	NVP	123–281	123–281	87–199	214–239	5–59 6–31	-
9	18 February	**45**, **90**	**44**, **95**, 143	147–344	147–344	104–243	219–233	17–59 2–38	63–76 108–160 84–96
10	19 February	33, 49, 65, 90	NVP	147–344	147–344	109–243	203–246	14–79 2–53 0–43 2–36	-

Note. No vertical propagations (NVPs) of gravity waves are found on 6, 16, and 19 February 2021. The time periods in bold fonts correspond to those with a match between the optical and the radio measurements within the temporal window of the Brunt-Väisälä period.
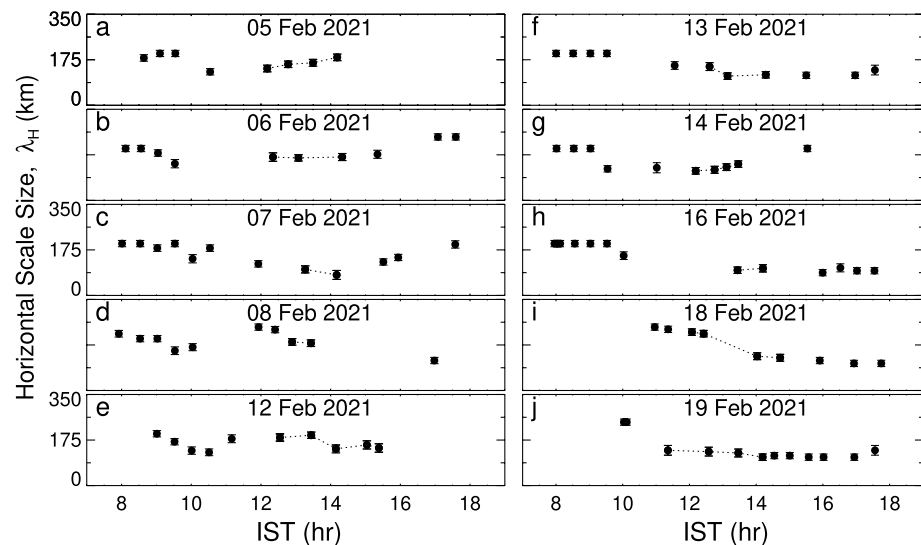
Figure 2. Diurnal variation of horizontal scale sizes of gravity waves for all the 10 days of bi-directional observation of dayglow emissions at OI 630.0 nm during 5–19 February 2021 are shown. The points joined by black-dotted line during noon-time correspond to those obtained by interpolating the values of λ_y before and after noon.

been described in an earlier study (Mandal et al., 2019). Several insightful results obtained with regard to gravity wave dynamics as a function of the seasons, solar flux variations, geomagnetic conditions, and day-to-day behavior have been reported in the literature (Mandal et al., 2020, 2022; Mandal & Pallamraju, 2020). In the present study, we have monitored the true height variations of constant electron densities corresponding to 5.0, 5.5, and 6.0 MHz transmission frequencies of digisonde, which has been shown in Figure 5a for a sample day of 5 February 2021. The phases can be seen to appear first in the higher heights, that is, in the variation of 6.0 MHz isoelectron density contours (red color) and they appear later in time in the case of 5.0 MHz contour (orange color). To aid the eye, black-dashed lines have been drawn for identification of downward phase movement. This kind of downward phase propagation is a characteristic property of upward propagating atmospheric gravity waves (Hines, 1960). Further, to ascertain that these phase offsets were indeed caused by an upward propagating gravity wave, time series analyses as described above are carried out for each of these isoelectron density contours for all the days of available data and are shown in Figure 5b. The Lomb-Scargle periodogram analysis shows the presence of multiple periods (66 and 94 min) in all three isoelectron density contours that are significant as can be
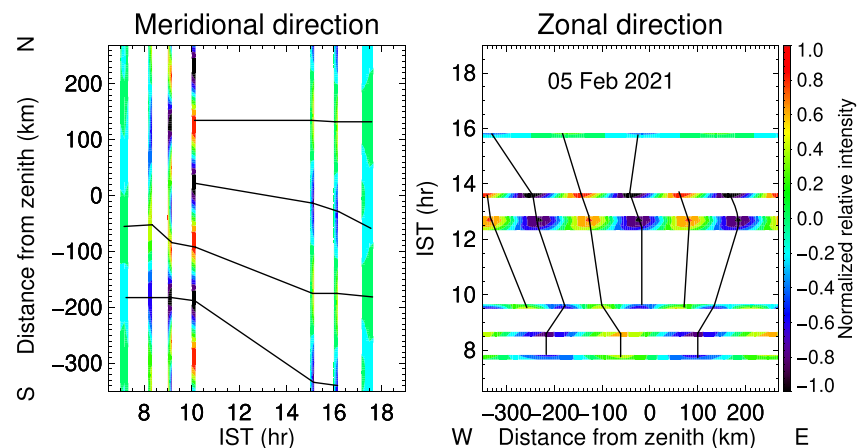

Figure 3. The normalized relative dayglow intensity variations obtained through inverse Fourier transform of a band centered on the dominant scale size are shown for a given day 5 February 2021. The left/right panels correspond to meridional/zonal directions. Black solid lines connect the crest/trough at one time to the other and aid the eye in the visualization of the movement of crests and troughs with time.
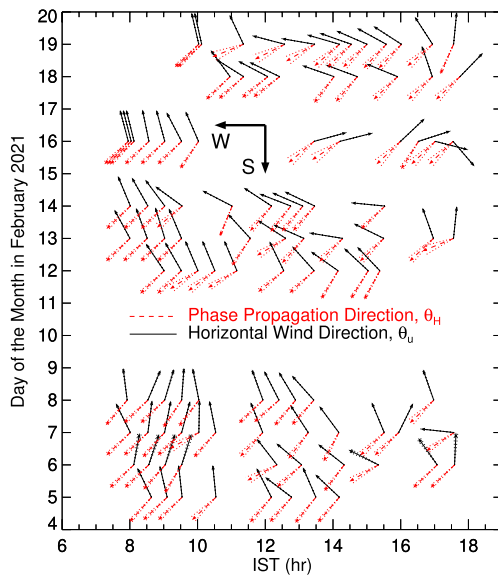
Figure 4. The time variation in propagation directions of the gravity waves for all the 10 days considered in this study are shown by red-dashed arrows and those for observed thermospheric winds by MIGHTI are presented in black-colored arrows.

seen in Figure 5b. As fluctuations of different temporal scales are superposed in the height variations of these isoelectron density contours, we filtered each of these contours for the particular gravity wave of time period of around 94 min. In this, the spectral power for this particular time period ±10 min window (corresponding to the Brunt-Väisälä period) is retained. For the rest of the frequencies, it is made zero. Then, the inverse Fourier transform is performed to obtain height variations in the isoelectron density contours only for that chosen common time period of the gravity waves. Figure 5c shows filtered variations in the heights of isoelectron density contours for a gravity wave of period 94 min on 5 February 2021. The downward phase propagation becomes more apparent in these filtered contours (as can be seen in Figure 5c). For time period of 66 min, such downward phase propagation was not seen in the filtered height variation in all the frequencies. We then use the height and time differences between crests and troughs of successive isoelectron density contours to calculate vertical propagation speeds of these gravity waves and vertical scale sizes (λ_z) by taking a product of the time periods and propagation speeds. On 5 February 2021, the λ_z of the gravity wave of time period 94 min is found to be varying in the range of 65–90 km. It is important and pertinent to note that this period of 94 min seen in the digisonde (Figure 5) data analysis is very close within the limit of the Brunt-Väisälä period (10 min) of the 101 min periodicity obtained from the optical data (Figure 1). This clearly strengthens the conjecture that the λ_x and λ_y obtained from optical data and the λ_z obtained from the digisonde data combinedly describe the three-dimensional behavior of the same gravity wave in the daytime. In this study, digisonde data have been analyzed for all
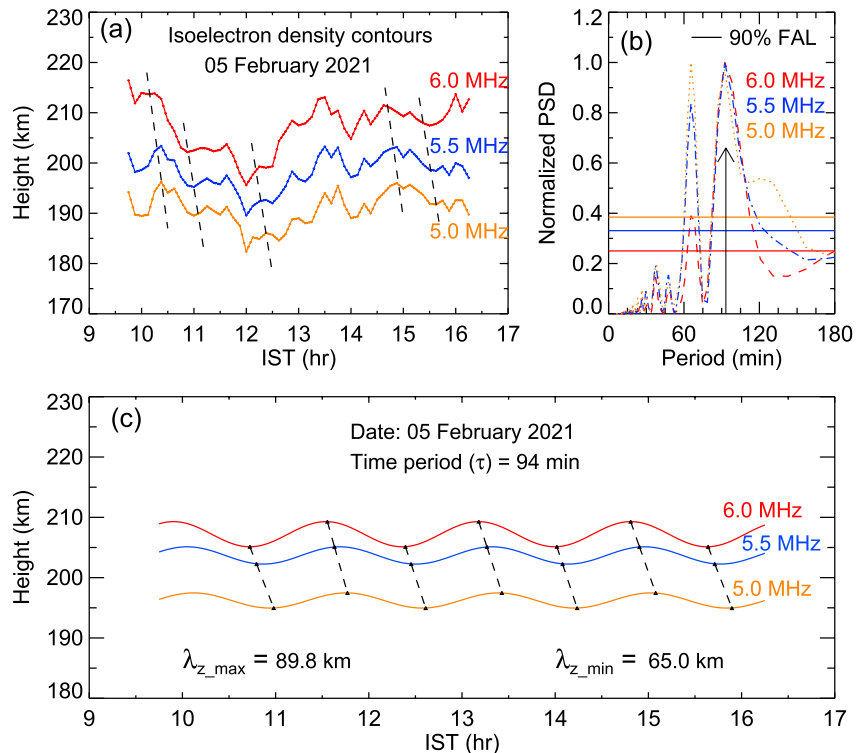

Figure 5. (a) Height variations of isoelectron densities corresponding to digisonde transmission frequencies of 5.0 (orange), 5.5 (blue), and 6.0 MHz (red). (b) The Lomb-Scargle periodogram of the isoelectron density height variations presented in (a), wherein a time period of 66 and 94 min are found to be significant and present in all of them. (c) Height variations of isoelectron density contours filtered for the gravity wave of time period of 94 min.

10 days of bi-directional mode of operation of optical data. Among the 10 days of data vertical propagation is seen to be existing on 7 days. In an earlier study (Mandal & Pallamraju, 2020), based on the analyses of 2 years of data, it has been shown that the vertical propagation of gravity waves is present on only around 40% of the days. This study revealed that although gravity waves are omnipresent, not on all days they propagate upwards as also seen from the results of the present study. In these seven days, the time periods and vertical wavelengths are found to be in the range of 37–143 min and 26–247 km, respectively (listed in Table 1). For a given day, only the time periods of gravity waves which showed vertical propagation are listed in the Table. The time periods in bold fonts correspond to those with a match between the optical and the radio measurements within the temporal window of the Brunt-Väisälä period. Thus, they combinedly are considered to represent the characteristics of the three-dimensional gravity wave on that day. Therefore, collocated and simultaneous optical and radio measurements, enable obtaining unique information on the horizontal and vertical propagation characteristics of the daytime thermospheric gravity wave.

4. Results

We have used the horizontal characteristics to estimate the vertical scale sizes of gravity waves. All the three-dimensional characteristics have been used to estimate horizontal winds. These estimates have been compared with the measured values and they are described in the sections below.

4.1. Estimation of Vertical Scale Sizes Using Gravity Wave Dispersion Relation

We used the gravity wave dispersion relation to estimate the gravity wave vertical scale sizes from the measured horizontal wave propagation characteristics as obtained by optical measurement. In the thermosphere, the strength of the wave dissipating factors such as molecular viscosity, thermal diffusivity, and ion-drag increase and cause dissipation of the upward propagating gravity waves. These forces are more prominent in the upper thermosphere above 300 km as shown in earlier studies (Fukao et al., 1993; Nicolls et al., 2012; Oliver et al., 1997; Vadas & Nicolls, 2012). Oliver et al. (1997) have shown that the thermospheric gravity wave characteristics obtained by the MU radar match with those of the non-dissipative gravity waves. They found that at around 500 km there are no downward phase propagations of gravity waves. Further, Nicolls et al. (2012) reported growth in amplitudes of the gravity waves with height in the altitude range of 200–300 km, which suggest that these gravity waves are not dissipating at these altitudes. In this work, we have used the OI 630.0 nm dayglow emission to study the horizontal propagation of thermospheric gravity waves and the peak emission altitude of this dayglow is around 230 km, which is in the non-dissipative region of gravity waves. Therefore, we have used the Hines' dispersion relation (Hines, 1960) of non-dissipating gravity waves for the estimation of vertical scale sizes of these observed gravity waves.

$$\omega_I^2 = k_H^2 \ast N^2/\left(k_H^2 + k_z^2 + 1/4H^2\right) \tag{2}$$

where, ω_I = intrinsic frequency, k_z = vertical wave number, and k_H = horizontal wave number of the gravity wave; H = scale height (=kT/mg, where k is the Boltzmann constant, T is neutral temperature, and m is the atomic mass); and N = Brunt-Väisälä frequency (=[$2g*/5H$]1/2, where g* is the gravitational acceleration at observation altitude).

The intrinsic and observed frequencies of the observed gravity waves are related as,

$$\omega_I = \omega - k_H .U \cos(\Delta\theta) \tag{3}$$

where ω = observed angular frequency; U = horizontal neutral wind; and $\Delta\theta$ = angle between the propagation directions of gravity waves and horizontal winds.

Here, we have used the values of ω, k_H, and θ_H obtained from the analyses of OI 630.0 nm dayglow data (refer to Figures 1, 2, and 4). The NRLMSISE-00 model-derived values corresponding to an altitude of 230 km over Ahmedabad have been used to calculate N and H. In addition to these, HWM14 model-derived (Drob et al., 2015) horizontal wind profiles (directions and magnitudes) corresponding to an altitude of 230 km over Ahmedabad, have been used as inputs in the dispersion relation (Equation 2). In this way, we have estimated the gravity wave vertical scale sizes throughout the day, whenever λ_H measurements are available. For comparison, such
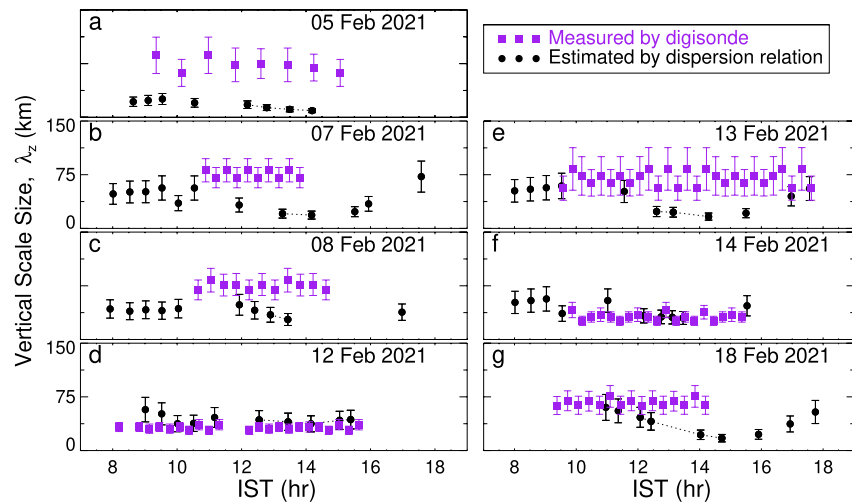
Figure 6. (a) Estimated values of λ_z from the dispersion relation are shown in black-circles and violet-squares are the measured values of λ_z from digisonde data for 5 February 2021. Panels (b–g) show the results as shown in Panel (a), but for 7, 8, 12, 13, 14, and 15 February 2021, respectively. The values connected by black-dotted lines represent those which have used interpolated λ_y values as described in the text.

estimations have been carried out for all 7 days, when measured values of λ_z are also available from collocated digisonde measurements. Also, these calculations have been carried out only for the common time periods, as observed in both optical and radio measurements (listed in Table 1 in bold fonts). These are presented in different panels in Figure 6 by black circles.

4.2. Comparison of Estimated Vertical Scale Sizes With Those Obtained From Digisonde Measurements

In Section 3.2, we have discussed the details of the digisonde data analyses to obtain vertical scale sizes (λ_z) of the upward propagating gravity waves. Thus, we have carried out a comparison of the estimated λ_z from the dispersion relation (as described in Section 4.1) with the measured values of λ_z as obtained from digisonde for all 7 days (Figure 6). Here, the violet-colored squares represent the measured values of λ_z resulted from the analyses of digisonde-derived isoelectron density contours (as discussed in Section 3.2). From this figure, one can appreciate the fact that the estimated λ_z values match reasonably well on some days with those measured independently from digisonde. However, there are days (5, 7, and 8 February) when the matching is not encouraging. One of the reasons could be that the model-derived winds and neutral atmospheric parameters may not accurately represent the upper atmospheric behavior on those days. Out of these two, the model-derived winds have a higher uncertainty in their values compared to the neutral atmospheric parameters. In a recent study, it has been shown that the optical dayglow emissions are influenced by the meridional (poleward) winds as they transport the constituents spatially (Kumar et al., 2022). Thus, this comparison serves as a motivation to explore the possibility of obtaining values of thermospheric neutral winds using the measured characteristics of gravity waves, information on which is very limited in the daytime. Such an effort has been carried out as described below and shown in the supplementary data.

4.3. Estimation of Thermospheric Neutral Winds

So far, we have seen that the vertical scale sizes estimated from gravity wave dispersion relation, match reasonably well on many occasions with those measured independently by radio technique. For the estimation of vertical scale sizes using the dispersion relation, we have used the HWM14 model-derived neutral winds which, being climatological in nature, is not expected to represent the true behavior of the atmosphere on a given day, especially, if there are some developments away from the normal. Nevertheless, in the present work, as we have with us the measured values of gravity wave parameters in all three dimensions, this presents a unique possibility of obtaining information on the ambient neutral winds. Thus, we have made such an attempt, wherein, the measured
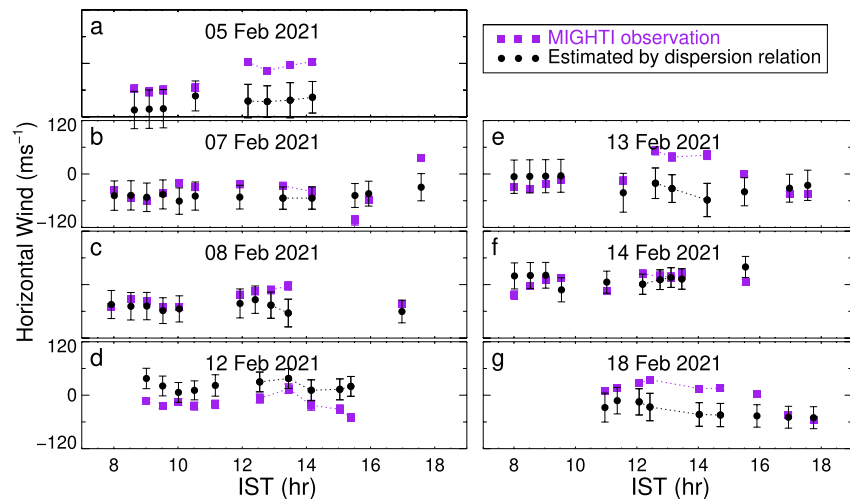
Figure 7. (a) Estimated horizontal wind magnitudes along the direction of wave propagation are shown by black-dotted line for 5 February 2021. Violet-colored squares represent the measured wind magnitudes along the wave propagation direction as obtained from the MIGHTI on-board ICON satellite. Panels (b–g) show the results as shown in Panel (a) but for 7, 8, 12, 13, 14, and 18 February 2021, respectively. The values joined by dotted lines correspond to those where λ_y values are interpolated as described in text.

values have been used, as inputs, into the gravity wave dispersion relation to obtain the thermospheric neutral winds. The results so obtained are discussed below.

All the measured horizontal and vertical propagation characteristics of gravity waves obtained by the collocated optical and radio observations are used as inputs in Equations 2 and 3 along with the NRLMSISE-00 model-derived neutral atmospheric parameters. Then these equations are solved for the wind values along the direction of wave propagations. Since the times corresponding to the measured values of λ_z from digisonde are different from those obtained for λ_H from optical data (as can be seen in Figure 6), the nearest measured λ_z value(s) have been considered for a given time in this calculation. The estimated wind magnitudes as a function of time for each of these days are shown in different panels as black-circles in Figures 7a–7g. Thus, by using this method, neutral winds in the direction of gravity propagation have been estimated.

4.4. Comparison of Neutral Wind Derived by the 3-D Gravity Waves With Measured MIGHTI Winds Onboard ICON

Recently, with the launch of the ICON satellite, thermospheric wind measurements became available through MIGHTI. This provides us with an opportunity to compare the estimated winds by the present method with those measured by MIGHTI. However, these measured winds cannot be readily used for comparison, as MIGHTI winds are not available for all times at a given location. Therefore, to obtain the diurnal variation of these measured neutral winds over our observational location, Ahmedabad, we have used a methodology described in one of our earlier works (Kumar et al., 2022). In this method, we use the HWM14 (Drob et al., 2015) model-derived winds to describe the climatological variations between the latitude of interest and the latitude of MIGHTI observations in a longitude region at a given time. We use the MIGHTI winds to provide the corrections to the HWM14 winds at the location of our interest. Thus, the difference between the HWM14 model winds and the observed MIGHTI winds for a given latitude of MIGHTI observation has been added to the HWM14 model-derived winds for a latitude of our interest.

In the present case, a $\pm 5°$ longitudinal region centered at Ahmedabad is considered and the latitudes at which MIGHTI winds are available at different times in that longitude region are noted. As mentioned above, the difference between the HWM14 and MIGHTI measured winds at that location is added to the HWM14 winds over Ahmedabad at a given time and thereby we obtain the diurnal variation in winds over Ahmedabad. This 'MIGHTI added HWM14 winds' method was successfully applied in the earlier study (Kumar et al., 2022) to obtain neutral winds over Ahmedabad, and interesting dynamics of meridional winds versus OI 630.0 nm dayglow emissions intensity variation were obtained. While this method provides neutral winds over Ahmedabad, for it to be

compared with the estimated winds in the present study, measured winds along the direction of wave propagation are required to be considered. For this, the cosine components of these winds are calculated along the direction of wave propagation using the measured angle between the wind and wave propagation directions as shown in Figure 4. Here, the wind propagation directions are calculated using the magnitude of zonal and meridional winds and are shown as black-colored arrows in Figure 4. In this way, the magnitude of measured thermospheric winds by MIGHTI on-board ICON satellite are calculated along the wave propagation directions and they are shown by violet-colored lines in Figures 7a–7g. It can be appreciated that these winds, derived through independent measurements: one estimated using the measured gravity wave parameters in three dimensions from collocated ground-based optical and radio measurements; and the other measured from the ICON satellite, show a very good match. Therefore, the characterization of gravity waves in three dimensions from ground-based measurements can be used to obtain a very good estimate of daytime thermospheric winds at a very high temporal resolution.

5. Discussion

We have presented a new approach and a new possibility of obtaining (a) vertical scale sizes of gravity waves in the daytime by using only the optical measurements (Section 4.1), and (b) thermospheric neutral winds by using coupled optical and radio measurements (Section 4.3). All these measurements and model outputs are independent of one another. The match in the parameters derived in the present study, namely, (a) estimated λ_z from the optical technique with the measured λ_z by radio technique (Section 4.2), and (b) estimated horizontal winds by the combined optical and radio measurements with the MIGHTI observed horizontal winds (Section 4.4), are remarkable. However, there are deviations in such comparison between the estimated and measured values of λ_z as noted on 5, 7, and 8 February 2021 (Figures 6a–6g) along with a few times on other days. It is well-known that the upper atmosphere is a highly dynamic and coupled system, with winds controlling the horizontal and vertical scale sizes of gravity waves. The neutral winds in the same/opposite direction of gravity wave propagation increase/decrease the horizontal scale sizes. Accordingly, the magnitude of vertical scale sizes decreases/increases (e.g., Mandal et al., 2019; Mandal & Pallamraju, 2020; Pallamraju et al., 2016; Vadas et al., 2009). Thus, horizontal propagation characteristics, which are used as inputs in gravity wave dispersion relation, are sensitive to surrounding wind fields. In this background, the differences between the estimated and measured values of λ_z on 5, 7, and 8 February 2021 could be understood as the estimated winds on 7 and 8 February, show a good match with measured winds from MIGHTI throughout the day. On 5 February, winds obtained by the two techniques match reasonably well except around noon-time. On some of the days (5, 13, and 18 February 2021), the values of estimated and measured winds around noon time as shown in Figure 7 do not match with each other. The possible reason of this difference could be that the λ_H and θ_H values in this duration were interpolated and not measured as discussed in Section 3.1. Nevertheless, by reducing the duration of optical observation in the zonal direction and carefully allowing a few meridional observations, this time gap can be reduced, which will be attempted in the future.

We further carried out an exercise to estimate λ_z using these measured winds instead of HWM14 model-derived winds. In that case, the estimated λ_z values have been found to show a good agreement with the measured ones (as shown in Figure S1). This further strengthens the discussion carried out in Section 4.2 that the locally varying neutral dynamics, do not get accurately described by the outputs of climatological models (HWM14 and NRLMSISE-00) at all times. This could be the probable source of deviations between the measured and estimated values of λ_z and winds on some occasions (Figures 6 and 7).

Here, one should note that it is not possible to estimate the neutral winds only by using optical measurements as there are two unknown parameters in the dispersion relation, namely, λ_z and time period, which need to be ascertained first. While various gravity wave parameters can be derived from the optical data and digisonde data independently, the key is to track the time period of gravity waves that are common in both optical and radio measurements. Attention is drawn to Table 1, wherein, the nearly similar values of time periods in the optical and radio measurements are listed in bold fonts, which are attributed to corresponding to the same wave. Thus, the gravity wave information obtained by the combined optical and radio measurements complement each other in describing the three-dimensional characteristics of gravity waves in the daytime from the ground-based measurements at an unprecedented temporal resolution. These describe the three-dimensional structure of the gravity wave characteristics accurately, which are also confirmed by the encouraging comparison between the horizontal winds derived by our measurements and those measured independently on-board ICON satellite. Results such as

these provide new directions for the investigation of the upper atmospheric neutral dynamics from ground-based measurements. These results and approach described assume a greater significance, as it is now possible to derive thermospheric neutral winds from ground-based techniques as this is a very challenging task, especially in daytime conditions. This result, to the best of our knowledge, is first of its kind, wherein the intriguing nature of interaction between the thermospheric neutral winds and gravity waves in the daytime has been demonstrated experimentally using high cadence ground-based experiments.

6. Summary

Detailed analyses of daytime airglow emission variations and digisonde-derived height profiles of electron densities have been carried out to characterize the thermospheric gravity waves in three dimensions in the daytime. Different parameters that characterize the atmospheric gravity waves are obtained/derived by using measurements, such as, time periods observed in the optical data, time periods observed in the radio data, λ_x, λ_y, λ_H, phase propagation angle from the east, estimated and measured λ_z are listed in Table 1. Out of the 10 days of bi-directional mode of operation of MISE, the vertical propagations of gravity wave are found to exist on 7 days. In this period, gravity wave parameters, such as, time period, θ_H, λ_x, λ_y, λ_H, and λ_z obtained from optical and radio measurements are found to be varying in the range of 31–138 min, 203°–248° from east, 88–344, 123–344, 78–243, and 26–247 km, respectively. Further, we have used these horizontal propagation characteristics of gravity waves obtained from large FOV optical measurements of OI 630.0 nm dayglow along with the model-derived winds and neutral atmospheric parameters to estimate the vertical scale sizes of these waves. The estimated vertical scale sizes show a reasonable match with those obtained from the analyses of digisonde-derived isoelectron density height variations. As the combined measurements describe the gravity wave in three-dimension very well, we have used all the measured wave parameters in the gravity wave dispersion relation to estimate the thermospheric neutral winds along the wave propagation direction. These estimated wind magnitudes show a reasonable match with those measured by MIGHTI added HWM14 model-derived winds. These results make the present work very unique, and it is expected that such findings on the daytime thermospheric neutral gravity waves and wind dynamics provide new directions and insights into the investigation of the upper atmospheric research.

Data Availability Statement

ICON data are processed in the ICON Science Data Center at UCB and available at https://icon.ssl.berkeley.edu/Data. The NRLMSISE-00 model-data are available at http://ccmc.gsfc.nasa.gov/modelweb/models/nrlmsise00.php. Text files needed to reproduce the figures presented in this paper can be accessed from: https://osf.io/rg3xs/.

References

Alexander, M. J. (1996). A simulated spectrum of convectively generated gravity waves: Propagation from the tropopause to the mesopause and effects on the middle atmosphere. *Journal of Geophysical Research*, *101*(D1), 1571–1588. https://doi.org/10.1029/95JD02046

Alexander, M. J., Beres, J. H., & Pfister, L. (2000). Tropical stratospheric gravity wave activity and relationships to clouds. *Journal of Geophysical Research: Atmosphere*, *105*(D17), 22299–22309. https://doi.org/10.1029/2000JD900326

Burnside, R., Herrero, F., Meriwether, J., Jr., & Walker, J. (1981). Optical observations of thermospheric dynamics at Arecibo. *Journal of Geophysical Research*, *86*(A7), 5532–5540. https://doi.org/10.1029/JA086iA07p05532

Djuth, F., Sulzer, M., Gonzales, S., Mathews, J., Elder, J., & Walterscheid, R. (2004). A continuum of gravity waves in the Arecibo thermosphere? *Geophysical Research Letters*, *31*(16), L16801. https://doi.org/10.1029/2003GL019376

Drob, D. P., Emmert, J. T., Meriwether, J. W., Makela, J. J., Doornbos, E., Conde, M., et al. (2015). An update to the horizontal wind model (HWM): The quiet time thermosphere. *Earth and Space Science*, *2*(7), 301–319. https://doi.org/10.1002/2014EA000089

Englert, C. R., Harlander, J. M., Brown, C. M., Marr, K. D., Miller, I. J., Stump, J. E., et al. (2017). Michelson interferometer for global high-resolution thermospheric imaging (MIGHTI): Instrument design and calibration. *Space Science Reviews*, *212*(1), 553–584. https://doi.org/10.1007/s11214-017-0358-4

Francis, S. H. (1973). Acoustic-gravity modes and large-scale traveling ionospheric disturbances of a realistic, disturbances of a realistic, dissipative atmosphere. *Journal of Geophysical Research*, *78*(13), 2278–2301. https://doi.org/10.1029/JA078i013p02278

Fritts, D. C. (1982). Shear excitation of atmospheric gravity waves. *Journal of the Atmospheric Sciences*, *39*(9), 1936–1952. https://doi.org/10.1175/1520-0469

Fritts, D. C. (1984). Shear excitation of atmospheric gravity waves. Part I: Non-linear radiation from a free shear layer. *Journal of the Atmospheric Sciences*, *41*(4), 524–537. https://doi.org/10.1175/1520-0469

Fritts, D. C., & Alexander, M. J. (2003). Gravity wave dynamics and effects in the middle atmosphere. *Review of Geophysics*, *41*(1), 1003. https://doi.org/10.1029/2001RG000106

Fukao, S., Yamamoto, Y., Oliver, W., Takami, T., Yamanaka, M., Yamamoto, M., et al. (1993). Middle and upper atmosphere radar observations of ionospheric horizontal gradients produced by gravity waves. *Journal of Geophysical Research*, *98*(A6), 9443–9451. https://doi.org/10.1029/92JA02846

Gerrard, A. J., & Meriwether, J. W. (2011). Initial daytime and nighttime SOFDI observations of thermospheric winds from Fabry-Perot Doppler shift measurements of the 630-nm OI line-shape profile. *Annales Geophysicae*, *29*(9), 1529–1536. https://doi.org/10.5194/angeo-29-1529-2011

Herrero, F., Mayr, H., & Spencer, N. (1988). Low latitude thermospheric meridional winds between 250 and 450 km altitude: AE-E satellite data. *Journal of Atmospheric and Terrestrial Physics*, *50*(10–11), 1001–1006. https://doi.org/10.1016/0021-9169(88)90087-6

Hickey, M., & Cole, K. (1988). A numerical model for gravity wave dissipation in the thermosphere. *Journal of Atmospheric and Terrestrial Physics*, *50*(8), 689–697. https://doi.org/10.1016/0021-9169(88)90032-3

Hines, C. O. (1960). Internal atmospheric gravity waves at ionospheric heights. *Canadian Journal of Physics*, *38*(11), 1441–1481. https://doi.org/10.1139/p60-150

Hocke, K., & K'ampfer, N. (2009). Gap filling and noise reduction of unevenly sampled data by means of the Lomb-Scargle periodogram. *Atmospheric Chemistry and Physics*, *9*(12), 4197–4206. https://doi.org/10.5194/acp-9-4197-2009.,

Hocke, K., & Schlegel, K. (1996). A review of atmospheric gravity waves and travelling ionospheric disturbances: 1982-1995. *Annales Geophysicae*, *14*(9), 917–940. https://doi.org/10.1007/s00585-996-0917-6.,

Immel, T. J., England, S., Mende, S., Heelis, R., Englert, C., Edelstein, J., et al. (2018). The ionospheric connection explorer mission: Mission goals and design, design. *Space Science Reviews*, *214*(1), 1–36. https://doi.org/10.1007/s11214-017-0449-2

Karan, D. K., & Pallamraju, D. (2017). Small-scale longitudinal variations in the daytime equatorial thermospheric wave dynamics as inferred from oxygen dayglow emissions. *Journal of Geophysical Research: Space Physics*, *122*(6), 6528–6542. https://doi.org/10.1002/2017JA023891

Karan, D. K., & Pallamraju, D. (2018). Effect of geomagnetic storms on the day-time low-latitude thermospheric wave dynamics. *Journal of Atmospheric and Solar-Terrestrial Physics*, *170*, 35–47. https://doi.org/10.1016/j.jastp.2018.02.003.,

Kumar, S., Pallamraju, D., Suryawanshi, P., Vijayalakshmi, T., & Seemala, G. K. (2022). On the latitudinal variation in oi 630.0 nm dayglow emissions in response to the equatorial electrodynamic processes and neutral winds. *Advances in Space Research*, *69*(2), 926–938. https://doi.org/10.1016/j.asr.2021.10.034

Lakshmi Narayanan, V., Gurubaran, S., & Emperumal, K. (2010). Airglow imaging observations of small-scale structures driven by convective instability in the upper mesosphere over Tirunelveli (8.7°N). *Journal of Geophysical Research: Atmospheres*, *115*(D19), D19119. https://doi.org/10.1029/2009JD012937

Laskar, F. I., Pallamraju, D., Veenadhari, B., Lakshmi, T. V., Reddy, M. A., & Chakrabarti, S. (2015). Gravity waves in the thermosphere: Solar activity dependence. *Advances in Space Research*, *55*(6), 1651–1659. https://doi.org/10.1016/j.asr.2014.12.040

Li, J., & Lu, X. (2021). Global responses of gravity waves and zonal mean winds to the madden-julian oscillation and the latitudinal dependence of their relations using MERRA-2. *Geophysical Research Letters*, *48*(20), e2021GL094717. https://doi.org/10.1029/2021GL094717

Lomb, N. R. (1976). Least-squares frequency analysis of unequally spaced data. *Astrophysics and Space Science*, *39*(2), 447–462. https://doi.org/10.1007/BF00648343

Makela, J. J., Fisher, D. J., Meriwether, J. W., Buriti, R. A., & Medeiros, A. F. (2013). Near-continual ground-based nighttime observations of thermospheric neutral winds and temperatures over equatorial Brazil from 2009 to 2012. *Journal of Atmospheric and Solar-Terrestrial Physics*, *103*, 94–102. https://doi.org/10.1016/j.jastp.2012.11.019

Mandal, S., & Pallamraju, D. (2020). Thermospheric gravity wave characteristics in the daytime over low-latitudes during geomagnetic quiet and disturbed conditions. *Journal of Atmospheric and Solar-Terrestrial Physics*, *211*, 105470. https://doi.org/10.1016/j.jastp.2020.105470

Mandal, S., Pallamraju, D., Karan, D., Phadke, K., Singh, R., & Suryawanshi, P. (2019). On deriving gravity wave characteristics in the daytime upper atmosphere using radio technique. *Journal of Geophysical Research: Space Physics*, *124*(8), 6985–6997. https://doi.org/10.1029/2019JA026723

Mandal, S., Pallamraju, D., & Pant, T. (2022). Vertical propagation speeds of gravity waves in the daytime as a precursor to the onset of the equatorial spread-f. *Journal of Geophysical Research: Space Physics*, *127*(8). https://doi.org/10.1029/2022JA030401

Mandal, S., Pallamraju, D., & Suryawanshi, P. (2020). Changes in the daytime thermospheric gravity wave propagation characteristics over low-latitudes in response to the variation in solar flux. *Journal of Atmospheric and Solar: Terrestrial Physics*, *209*, 105414. https://doi.org/10.1016/j.jastp.2020.105414

Medvedev, A., & Klaassen, G. (2000). Parameterization of gravity wave momentum deposition based on nonlinear wave interactions: Basic formulation and sensitivity tests. *Journal of Atmospheric and Solar-Terrestrial Physics*, *62*(11), 1015–1033. https://doi.org/10.1016/S1364-6826(00)00067-5

Meriwether, J., Jr., Moody, J., Biondi, M., & Roble, R. (1986). Optical interferometric measurements of nighttime equatorial thermospheric winds at Arequipa, Peru. *Journal of Geophysical Research*, *91*(A5), 5557–5566. https://doi.org/10.1029/JA091iA05p05557

Miyoshi, Y., Fujiwara, H., Jin, H., & Shinagawa, H. (2014). A global view of gravity waves in the thermosphere simulated by a general circulation model. *Journal of Geophysical Research: Space Physics*, *119*(7), 5807–5820. https://doi.org/10.1002/2014JA019848

Nicolls, M., Vadas, S., Meriwether, J., Conde, M., & Hampton, D. (2012). The phases and amplitudes of gravity waves propagating and dissipating in the thermosphere, thermosphere: Application to measurements over Alaska. *Journal of Geophysical Research: Space Physics*, *117*(A5). https://doi.org/10.1029/2012JA017542

Oliver, W. L., Fukao, S., Yamamoto, Y., Takami, T., Yamanaka, M. D., Yamamoto, M., et al. (1994). Middle and upper atmosphere radar observations of ionospheric density gradients produced by gravity wave packets. *Journal of Geophysical Research*, *99*(A4), 6321–6329. https://doi.org/10.1029/94JA00171

Oliver, W. L., Otsuka, Y., Sato, M., Takami, T., & Fukao, S. (1997). A climatology of F region gravity wave propagation over the middle and upper atmosphere radar, radar. *Journal of Geophysical Research*, *102*(A7), 14499–14512. https://doi.org/10.1029/97JA00491

Pallamraju, D., Baumgardner, J., & Chakrabarti, S. (2002). Hirise: A ground-based high-resolution imaging spectrograph using echelle grating for measuring daytime airglow/auroral emissions (Vol. *64*). https://doi.org/10.1016/S1364-6826(02)00095-0

Pallamraju, D., Baumgardner, J., Chakrabarti, S., & Pedersen, T. R. (2001). Simultaneous ground based observations of an auroral arc in daytime/twilighttime OI, OI 630.0 nm emission and by incoherent scatter radar. *Journal of Geophysical Research*, *106*(A4), 5543–5549. https://doi.org/10.1029/2000JA000244

Pallamraju, D., Baumgardner, J., Singh, R. P., Laskar, F. I., Mendillo, C., Cook, T., et al. (2014). Daytime wave characteristics in the mesosphere lower thermosphere region: Results from the balloon-borne investigations of regional-atmospheric dynamics experiment. *Journal of Geophysical Research: Space Physics*, *119*(3), 2229–2242. https://doi.org/10.1002/2013JA019368

Pallamraju, D., & Chakrabarti, S. (2006). Contributions of imaging echelle spectrographs to daytime optical aeronomy. *Journal of Atmospheric and Solar-Terrestrial Physics*, *68*(13), 1459–1471. https://doi.org/10.1016/j.jastp.2005.05.013

Pallamraju, D., Das, U., & Chakrabarti, S. (2010). Short-and long-timescale thermospheric variability as observed from oi 630.0 nm dayglow emissions from low latitudes. *Journal of Geophysical Research*, *115*(A6). https://doi.org/10.1029/2009JA015042

Pallamraju, D., Karan, D. K., & Phadke, K. A. (2016). First three dimensional wave characteristics in the daytime upper atmosphere derived from ground-based multiwavelength oxygen dayglow emission measurements. *Geophysical Research Letters*, *43*(11), 5545–5553. https://doi.org/10.1002/2016GL069074

Pallamraju, D., Laskar, F. I., Singh, R. P., Baumgardner, J., & Chakrabarti, S. (2013). MISE: A multiwavelength imaging spectrograph using echelle grating for daytime optical aeronomy investigations. *Journal of Atmospheric and Solar-Terrestrial Physics*, *103*, 176–183. https://doi.org/10.1016/j.jastp.2012.12.003

Pitteway, M. L. V., & Hines, C. O. (1963). The viscous damping of atmospheric gravity waves. *Canadian Journal of Physics*, *41*(12), 1935–1948. https://doi.org/10.1139/p63-194

Pramitha, M., Venkat Ratnam, M., Taori, A., Krishna Murthy, B., Pallamraju, D., & Vijaya Bhaskar Rao, S. (2015). Evidence for tropospheric wind shear ex-citation of high-phase-speed gravity waves reaching the mesosphere using the ray-tracing technique. *Atmospheric Chemistry and Physics*, *15*(5), 2709–2721. https://doi.org/10.5194/acp-15-2709-2015

Raghavarao, R., Sridharan, R., Sastri, J. H., Agashe, V. V., Rao, B. C. N., Rao, P. B., & Somayajulu, V. V. (1988). *The equatorial ionosphere; wits handbook world ionosphere/thermosphere study* (Vol. 1). SCOSTEP Secretariat, University of Illinois,

Richmond, A. (1978). Gravity wave generation, propagation, and dissipation in the thermosphere. *Journal of Geophysical Research*, *83*(A9), 4131–4145. https://doi.org/10.1029/ja083ia09p04131

Sato, K., Hashiguchi, H., & Fukao, S. (1995). Gravity waves and turbulence associated with cumulus convection observed with the uhf/vhf clear-air Doppler radars. *Journal of Geophysical Research*, *100* (D4), 7111–7119. https://doi.org/10.1029/95JD00198

Scargle, J. D. (1982). Studies in astronomical time series analysis. II-Statistical aspects of spectral analysis of unevenly spaced data. *The Astrophysical Journal*, *263*, 835–853. https://doi.org/10.1086/160554

Shepherd, G. G., Thuillier, G., Gault, W., Solheim, B., Hersom, C., Alunni, J., et al. (1993). Windii, the wind imaging interferometer on the upper atmosphere research satellite. *Journal of Geophysical Research*, *98*(D6), 10725–10750. https://doi.org/10.1029/93JD00227

Shiokawa, K., Otsuka, Y., & Ogawa, T. (2009). Propagation characteristics of night-time mesospheric and thermospheric waves observed by optical mesosphere thermosphere imagers at middle and low latitudes. *Earth Planets and Space*, *61*, 479–491. https://doi.org/10.1186/bf03353165

Singh, R. P., & Pallamraju, D. (2016). Effect of cyclone Nilofar on mesospheric wave dynamics as inferred from optical nightglow observations from Mount Abu, India. *Journal of Geophysical Research*, *121*(6), 5856–5867. https://doi.org/10.1002/2016JA022412

Smith, A. K., & Lyjak, L. V. (1985). An observational estimate of gravity wave drag from the momentum balance in the middle atmosphere. *Journal of Geophysical Research*, *90*(D1), 2233–2241. https://doi.org/10.1029/JD090iD01p02233

Solomon, S. C., & Abreu, V. J. (1989). The 630 nm dayglow. *Journal of Geophysical Research: Space Physics*, *94*(A6), 6817–6824. https://doi.org/10.1029/JA094iA06p06817

Taylor, M. J., Bishop, M. B., & Taylor, V. (1995). All-sky measurements of short period waves imaged in the OI(557.7 nm), Na(589.2 nm) and near infrared OH and $O_2(0, 1)$ nightglow emissions during the aloha-93 campaign. *Geophysical Research Letters*, *22*(20), 2833–2836. https://doi.org/10.1029/95GL02946

Teitelbaum, H., Massebeuf, M., Fellous, J., Petitdidier, M., Christophe, J., & Blanco, F. (1981). Simultaneous measurements of meteor winds and green line intensity variations: Gravity waves and planetary waves. *Journal of Geophysical Research: Space Physics*, *86* (A9), 7767–7770. https://doi.org/10.1029/JA086iA09p07767

Vadas, S. (2007). Horizontal and vertical propagation and dissipation of gravity waves in the thermosphere from lower atmospheric and thermospheric sources. *Journal of Geophysical Research*, *112*(A6). https://doi.org/10.1029/2006JA011845.,

Vadas, S., & Fritts, D. C. (2004). Thermospheric responses to gravity waves arising from mesoscale convective complexes. *Journal of Atmospheric and Solar-Terrestrial Physics*, *66*(6–9), 781–804. https://doi.org/10.1016/j.jastp.2004.01.025

Vadas, S., Fritts, D. C., & Alexander, M. J. (2003). Mechanism for the generation of secondary waves in wave breaking regions. *Journal of the Atmospheric Sciences*, *60*(1), 194–214. https://doi.org/10.1175/1520-0469

Vadas, S., & Liu, H.-l. (2009). Generation of large-scale gravity waves and neutral winds in the thermosphere from the dissipation of convectively generated gravity waves. *Journal of Geophysical Research*, *114*(A10). https://doi.org/10.1029/2009JA014108

Vadas, S., & Nicolls, M. (2012). The phases and amplitudes of gravity waves propagating and dissipating in the thermosphere: Theory. *Journal of Geophysical Research*, *117*(A5). https://doi.org/10.1029/2011JA017426

Vadas, S., Yue, J., She, C.Y., Stamus, P. A., Liu, A. Z., Liu, H. L., et al. (2009). A model study of the effects of winds on concentric rings of gravity waves from a convective plume near Fort Collins on 11 May 2004. *Journal of Geophysical Research*, *114*(D6), D06104. https://doi.org/10.1029/2008JD011244

VanderPlas, J. T. (2018). Understanding the lomb–scargle periodogram. *The Astrophysical Journal - Supplement Series*, *236*(1), 16. https://doi.org/10.3847/1538-4365/aab76

Yiğit, E., Aylward, A. D., & Medvedev, A. S. (2008). Parameterization of the effects of vertically propagating gravity waves for thermosphere general circulation models: Sensitivity study. *Journal of Geophysical Research*, *113*(D19), D19106. https://doi.org/10.1029/2008JD010135

Yiğit, E., & Medvedev, A. S. (2009). Heating and cooling of the thermosphere by internal gravity waves. *Geophysical Research Letters*, *36*(14), L14807. https://doi.org/10.1029/2009GL038507